

# 1 Permeability, Selectivity and Distinguishing Criterion of Silicone Membrane 2 for Supercritical CO<sub>2</sub> and N<sub>2</sub> in the Porous Media

3 Luqman K. Abidoye<sup>1,2</sup>, Diganta B. Das

4 Chemical Engineering Department, Loughborough University, Loughborough, Leicestershire  
5 LE11 3TU, United Kingdom

6  
7 <sup>1</sup>Current address: Department of Civil Engineering, Osun State University, PMB 4494, Osogbo,  
8 Nigeria

9  
10 <sup>2</sup>Corresponding author; Email: [kluqman2002@yahoo.co.uk](mailto:kluqman2002@yahoo.co.uk); Phone: +2348142486988

## 11 12 Abstract

13 The possibility of leakage of CO<sub>2</sub> from the geological storage reservoir is of serious concern to  
14 stakeholders. In this work, high–pressure-temperature laboratory experiments were performed  
15 to demonstrate the application of a silicone membrane-sensor system in the monitoring of  
16 subsurface gases, especially in the leakage scenario. Mass permeation, membrane resistance  
17 to gas permeation and the gas flux across the membrane are reported for two gases, namely,  
18 CO<sub>2</sub> and N<sub>2</sub>. Mass permeation of CO<sub>2</sub> through the membrane was more than ten times higher  
19 than that of N<sub>2</sub>, under similar conditions. It was also found to increase with the geological  
20 depths. The gas flux remains higher for CO<sub>2</sub> as compared to N<sub>2</sub>. From the results, a simple  
21 criterion for distinguishing the presence of the different gases at various geological depths was  
22 formulated based on the rate of mass permeation of gas through the membrane. Results and  
23 techniques in this work can be employed in the detection/monitoring of subsurface gas  
24 movement, especially in geological carbon sequestration.

25  
26 **Keywords:** CO<sub>2</sub>, geological sequestration, leakage, monitoring, silicone rubber membrane.

## 27 1. Introduction

28 Global warming problems arising from climate change [1] have led to the practice of geological  
29 carbon sequestration so as to limit the amount of greenhouse gases in the atmosphere [2, 46,  
30 47]. However, the possibility of CO<sub>2</sub> leakage from geological carbon sequestration storage  
31 reservoir is a major concern to many stakeholders [3], [4]. This is because the leakage of CO<sub>2</sub>  
32 from the storage reservoir may pose serious danger to potable water aquifers that may lie along  
33 the CO<sub>2</sub> migration path. It also poses hazards to human and plant lives if the CO<sub>2</sub> finds its way  
34 to the earth's surface. Leakage of CO<sub>2</sub> may give rise to hazards to the marine lives if it leaks  
35 through the ocean leading to water acidification [5]. These possibilities and their adverse effects

36 hinder public acceptance and investors' confidence in the long term safety of the CO<sub>2</sub>  
37 sequestration process [4], [6].

38  
39 The safety of a CO<sub>2</sub> storage system can be compromised as a result of gravity override and/or  
40 viscous instability in the porous media initially filled with brine [7], [8]. This causes the CO<sub>2</sub> to  
41 move to the top of the injection layer and bypass large quantities of brine in the storage aquifer  
42 [9–11]. Similarly, wettability alteration of the caprock can lead into the migration of the CO<sub>2</sub>  
43 through overlying caprock [12–14], which can lead into the leakage of CO<sub>2</sub>. Overcoming these  
44 challenges requires the design of efficient sequestration processes, together with the effective  
45 monitoring strategies.

46  
47 Existing monitoring technologies for carbon sequestration are generally built upon the  
48 measurements of physico-chemical properties of the CO<sub>2</sub>-brine-rock system or the detectability  
49 of the reaction by-products, e.g., precipitation of carbonates in limestone-rich aquifer [15].  
50 Electromagnetic techniques [16], infrared monitoring [17], and temperature signals [18] have  
51 been demonstrated either in the laboratory or pilot applications for subsurface monitoring of  
52 gases. Methods, such as electromagnetic techniques utilise large differences in the values of  
53 the dielectric permittivities of CO<sub>2</sub> and water to establish contrasts between the original and  
54 current amounts of water and CO<sub>2</sub> at any time in the domain [19]. Near surface monitoring  
55 involves the analysis of near surface water, air and soil samples on a regular [20]. Numerical  
56 simulations [48, 49] have also shown the possibilities of CO<sub>2</sub> migration in the subsurface and its  
57 reactivity with underground minerals.

58  
59 Looking at the above-listed techniques, one may draw the conclusion that a number of  
60 techniques are already proposed for the monitoring of the carbon sequestration process.  
61 However, the costs of the instruments involved in the above techniques as well as the  
62 complexity of their operations and set up are often difficult tasks. This view was shared by  
63 Zimmer et al. [21]. These authors state that the conventional techniques for porous media gas  
64 sampling are time consuming, expensive, or limited in temporal sampling density and volume.  
65 In addressing the above issues, the potential of silicone rubber as a low-cost membrane for the  
66 monitoring of the presence of gas in the porous media is examined in this paper. Silicone  
67 rubber is a widely used elastomer in a wide range of industries. It is also one of the most gas  
68 permeable elastomers [22]. The high permeability of silicone rubber to gas is due to the high  
69 flexibility of silicone-oxygen chain, which enables easy diffusion of gas molecules. This property  
70 of silicone rubber has been exploited in gas separation, drug delivery, blood oxygenation and so  
71 on [23].

72 Earlier, Zimmer et al. [21] and Lazik et al. [24] demonstrated the applicability of silicone rubber  
73 as a membrane in the detection of gases present in the underground and boreholes.  
74 Investigations by Zimmer et al. [21] were connected to the geological carbon sequestration  
75 project (CO<sub>2</sub>SINK) in Ketzin, Germany. They have successfully demonstrated the detection of  
76 CO<sub>2</sub> front at observation wells, located at different distances to the injection well, using the gas  
77 membrane sensor that includes the silicone rubber. However, the analyses of the gases  
78 through the device rely on the mass spectrometer located on the ground surface, making the  
79 system complex and expensive to use. This however raises a question, i.e., whether or not a  
80 low-cost membrane-sensor system can be effectively applied in the monitoring of subsurface  
81 gas migration under high pressure and temperature conditions, as found in the geological  
82 carbon sequestration. As shown in the works of Cheng and Luo [25] and Zimmer et al. [21],  
83 there are many gases that can migrate in the subsurface apart from CO<sub>2</sub>. Considering the  
84 scenario where unknown gas possibly permeates into the membrane-sensor system, how can  
85 we possibly distinguish the presence of a particular gas in the subsurface using such a system?

86 To respond to these questions, this work attempts to characterize the performances of flat sheet  
87 silicone rubber devised with a pressure sensor for the detection of CO<sub>2</sub> and N<sub>2</sub> in porous media.  
88 Previously, Lazik et al. [24] demonstrated the application of membrane-sensor system in the  
89 continuous monitoring of O<sub>2</sub> and CO<sub>2</sub> in a sand-filled Lysimeter. However, they used tubular  
90 membrane unlike the flat-sheet membrane used in this work. The tubular nature of the  
91 membrane used in their work seems to make the measurement of the gas concentration more  
92 tedious unlike the straightforward measurement obtained in this work. This is because the  
93 tubular membrane required sensors with tubular geometry to achieve the measurement  
94 objective. Furthermore, the authors [24] show that the subsurface gas concentration can be  
95 determined by simple measurement of physical quantities (e.g., pressure or volume) only. This  
96 principle was utilised in this work by the measurement of the pressure of the gas that  
97 permeated through the membrane into the measurement chamber of the membrane-sensor  
98 system.

99 In our investigations, N<sub>2</sub>, as one of the abundant gases in the subsurface [26], is included as a  
100 model gas to create comparison for the responses of the membrane-sensor system to the  
101 presence of different gases. The characterization will be done in terms of the mass permeation  
102 of the gases through the membrane, dynamic profiles of gas fluxes across the membrane and  
103 membrane resistance to gas permeation. This work will utilize the differences in the  
104 performances of the membrane-sensor system under the influences of the different gases to  
105 establish distinguishing criterion for real-time monitoring of the gas migration in the subsurface.

106 The experiments involved the preparation of a porous domain with well-characterised silica  
107 sand particles. The domain boundary was made of steel cell to withstand the high pressure and

108 temperature conditions, applicable to geological carbon sequestration. A flat sheet silicone  
109 rubber was fitted into a steel holder together with a pressure transducer (sensor). This  
110 arrangement constitutes a membrane-sensor system, which was attached to the port at the  
111 centre of the wall of the porous domain. The experiments were designed to mimic the  
112 conditions of temperature and pressure that can be encountered by gases escaping from  
113 shallow subsurface. According to Best [27], the geobaric gradient in the continental crust is  
114 around 270 bar/km while geothermal gradients were reported to be 45 and 25°C/km for the  
115 warm and cold basins, respectively [28], [29]. In this work, warm basin is considered, and the  
116 calculated conditions for different geological depths, based on the above reports, were used to  
117 design the experiments. This work serves as a follow-up to our earlier publication [30], in which  
118 multiple techniques (e.g., pH, dielectric constant, bulk electrical conductivity and membrane flux  
119 parameter) were simultaneously demonstrated for use in the monitoring of potable water aquifer  
120 contaminated by leaked CO<sub>2</sub> at different geological depths.

## 121 **2. Materials and methods**

### 122 **2.1 Porous domain and materials**

123 The porous domain used in this work was prepared using commercially available silica sand  
124 particles. The domain was used to represent a geological structure while attempts were made  
125 to mimic the real conditions corresponding to different geological depths. The silica sand (DA  
126 14/25) was purchased from Minerals Marketing (Buxton, UK). Before use, the particles were  
127 pre-treated by washing in deionised water to remove any clay content and dried for at least 24  
128 hours. The bulk physical properties of the silica sand (porous domain) were determined in our  
129 laboratory. Constant-head permeameter technique [31] was used to determine the permeability  
130 of the porous domain to water. The experimentally determined physical and chemical properties  
131 of the samples are listed in Tab. 1. The silicone rubber sheet (part number: RS 340-2689) used  
132 in our experiments was obtained from RS Components Ltd (Northants, UK). The sheet has an  
133 average thickness of 3mm. The gases used were high purity CO<sub>2</sub> and N<sub>2</sub>, which were obtained  
134 from BOC Industrial Gases (Loughborough, UK).

### 135 **2.2 Instruments and sample holder set up**

136 The pressure of the gas that permeated through the silicone rubber membrane was measured  
137 with the HySense PR 140 pressure transducer (Hydrotechnik, GmbH, Holzheimer Strasse,  
138 Germany) with operating pressure of 0 to 100 bar. The head of the pressure transducer (PT)  
139 was fitted into locally manufactured steel holder that also holds the silicone rubber membrane in  
140 a tight position. Fig.1 shows the photograph of the sample holder filled with sand, and the steel  
141 holder, which holds the membrane and the pressure transducer (sensor). The silicone  
142 membrane was cut to the appropriate diameter to fit into the steel holder with the average

143 diameter of the membrane being  $7.3 \times 10^{-3}$  m while the infiltration area available for permeation  
144 is  $3.8 \times 10^{-3}$  m in diameter. The reason for the reduction in diameter for effective permeation  
145 was the metal cap on the top of the holder, which screwed down the membrane against a  
146 sintered metal disc at its base.

147  
148 The sample holder is a stainless steel cell with sample height of 4cm and 10cm diameter. The  
149 configuration of the sample holder with Pressure Transducers (PT) as well as interfacing with  
150 computer system for data collection and processing was described by [30] The gap between  
151 the membrane in the steel holder and the face of the PT at the base of the steel holder provides  
152 the space for the accumulation of gas that permeates through the membrane. This space has  
153 an average volume of  $1 \times 10^{-6}$  (m<sup>3</sup>). The pressure transducers were calibrated using a portable  
154 pressure calibrator, DPI 610 (Druck Limited, Leicester, UK). Electric heaters were located at the  
155 convenient corners of the heating cabinet and the system temperature was regulated using PID  
156 temperature controller (West Control Solutions, Brighton, UK). Readings were collected every  
157 10 s.

158  
159 Fig. 2 is a schematic diagram of the experimental set up. The figure illustrates the sample  
160 holder, the positions of the PTs. Narrow steel tubes run upstream and downstream of the cell  
161 with inlet for scCO<sub>2</sub> via the upstream tube connected to the supercritical fluid pump. The outlet  
162 pipe from the bottom of the sample holder has a metering valve (Swagelok, Kings Langley, UK)  
163 to shut or control outflow from the sample holder. In all experiments, it was shut to prevent the  
164 leakage of the gas in the sample holder. Furthermore, to ensure that there is no gas leakage  
165 and that the system is at the desired pressure, a precision backpressure regulator, BPR  
166 (Equilibar, Fletcher, NC, USA) is located further down the outlet tube. The back pressure  
167 regulator is a dome loaded type using peek materials as diaphragm and was loaded with  
168 nitrogen gas (BOC Industrial Gases, Loughborough, UK) from a cylinder with appropriate gas  
169 regulator (Gas-Arc Group Ltd, Norfolk, UK). The pressure imposed on the porous domain from  
170 the supercritical fluid pump was recorded by a CR10X data logger (Campbell Scientific,  
171 Shepshed, UK).

172

### 173 2.3 Experimental design

174 Geological sequestration of CO<sub>2</sub> can take place at depth of 1km or more [3], [32]. However,  
175 migration of leaked CO<sub>2</sub> from the storage aquifer may occur through several geological  
176 sediments, situated at different depths that lie above the storage aquifer, before reaching the  
177 earth's surface. Based on this scenario, our experiments were designed to mimic the presence  
178 of CO<sub>2</sub> at the hypothetical geological depths above the storage aquifer. As pointed out in the  
179 introductory part of this work, the reports of Best [27] and Nordbotten et al. [28] were used to

180 determine the pressure and temperature, respectively at the hypothetical geological depths for  
181 the experiments. Conditions at various geological depths, which were considered in this work,  
182 are listed in Tab. 2. For safety concerns during our experiments, the experimental conditions  
183 were chosen up to the limit of 300m depth. Fresh samples of silicone rubber membranes were  
184 used at the start of each experiment. At the start of the experiment, equipment was set up by  
185 placing the body of the sample holder on the bottom end piece (base cover or lid). Ports on the  
186 sample holder were plugged with steel holders, which hold the PTs and the membrane. These  
187 were then connected to the peripheral devices as discussed above for the automatic collection  
188 and logging of data. The silica sand was poured through a metal sieve of appropriate size with  
189 regular tamping to ensure uniform sand deposition. Equal amount of sand (500g) was used in  
190 all experiments.

191  
192 Then, the top end piece was placed in position. The weight of the top end piece compressed  
193 the sand to conditions suitable for high-pressure system. After tightening all the tubing joints,  
194 pressure was imposed on the BPR from the N<sub>2</sub> cylinder. The peek diaphragm in the BPR  
195 prevents the passage of the N<sub>2</sub> through the downstream tubing into the porous domain. The  
196 sample holder and some portions of the tubing were contained within a heating cabinet fitted  
197 with electric heaters. The heaters were turned on and set at the appropriate temperature for the  
198 experiment. A supercritical fluid pump (Teledyne Isco, Lincoln, USA) was filled with liquid CO<sub>2</sub>  
199 from the cylinder by opening of the valve, v-1, and setting the pump on refill mode. Following  
200 this, v-1 was closed and the supercritical fluid pump was set at the experimental pressure. This  
201 procedure supplied the CO<sub>2</sub> to the tubing from the exit of the supercritical fluid pump up to the  
202 valve, v-3 (see Fig.2).

203  
204 **Figure 1**  
205  
206 Constant pressure mode of the supercritical fluid pump was used throughout all the  
207 experiments. This mode imposed constant pressure of gas on the porous domain. When the  
208 temperature in the heating cabinet had reached the target condition, v-3 was opened and CO<sub>2</sub>  
209 was supplied into the sand in the sample holder. The pump being in constant pressure mode,  
210 any pressure fluctuation owing to the opening of the v-3 was quickly eliminated. The experiment  
211 continued for varying number of hours as convenient for the investigators. Measurements were  
212 performed at different temperatures and pressures following the conditions listed in Tab. 2. In  
213 addition, for each experiment, the result presented was the arithmetic average of the readings  
214 from the two sensors. The silicone rubber used in this work is a non-porous flat sheet  
215 membrane. Gas permeates the membrane by diffusion under the influence of the driving force,  
216 e.g., the pressure difference across the membrane. Commonly, concentration gradient is  
217 normally taken as the driving force in the permeation of gas through a membrane in the mixture

218 of gases (see, e.g., [24]). In this work, only pure gas was used in each experiment. Therefore,  
219 pressure gradient across the membrane is rightly considered to be the driving force. However,  
220 the emphasis in this work is to show the behaviour of different gases at different geological  
221 depths. As the depth is also strongly related to temperature and pressure, the emphasis on  
222 depth, in this work, can be directly related to the monitoring of gas movement in geological  
223 media at different positions. Fresh and used silicone rubber membranes scanned with the  
224 field emission gun scanning electron microscopy (FEGSEM) (LEO 1530VP, Carl Zeiss SMT,  
225 Oberkochen, Germany) are shown in Fig.3. No significant pores were detected in the  
226 membrane by the scan after the CO<sub>2</sub> permeation.

227  
228 For the experiments involving N<sub>2</sub>, the N<sub>2</sub> gas was supplied from the N<sub>2</sub> cylinder via the BPR.  
229 Here, v-3 was closed to prevent N<sub>2</sub> from entering the supercritical fluid pump. The diaphragm on  
230 the BPR was removed to provide a path for the N<sub>2</sub> to enter into the sand in the domain through  
231 the downstream tubing. The N<sub>2</sub> pressure was set on the gas regulator on top of the N<sub>2</sub> cylinder.  
232 All other procedures remained as defined above for the CO<sub>2</sub> experiments.

233

234 **Figure 2**

235

236 **Figure 3**

237

## 238 2.4 Calculation methods

239 The pressure reading at different time was used to determine the mass of the gas in the  
240 measurement chamber of the membrane-sensor system. In order to obtain real  
241 properties of the gases, Van der Waals equation was used to determine the mole of the  
242 gases. The mass of the gas was obtained from their respective mole at different time.  
243 Van der Waals equation is shown in Eq. (1):

$$244 [P + (n^2 a / V^2)](V - nb) = nRT \quad (1)$$

245  $P$  (Pa),  $n$  (mol),  $V$  (m<sup>3</sup>) and  $T$  (K) are the pressure, number of mole, volume and temperature,  
246 respectively, of the gas in the measurement chamber of the membrane-sensor system.  $R$  (J/mol  
247 K) is the universal gas constant,  $a$  (kg m<sup>5</sup>/s<sup>2</sup>mol<sup>2</sup>) and  $b$  (m<sup>3</sup>/mol) are constants, which fit the  
248 experiment closely to individual gas molecule. The mole,  $n$ , is obtained from equation (1) by  
249 approximating  $V$  in the term  $n^2 a / V^2$  (see, Eq. 1) using the ideal gas equation (i.e.,  $V = nRT/P$ ).  
250 After rearrangement,  $n$  is obtained as:

$$251 n = \frac{V(PR^2T^2 + aP^2)}{bPR^2T^2 + baP^2 + R^3T^3} \quad (2)$$

252 The mass,  $m$ , of the gas was obtained by multiplying the mole,  $n$ , with the molar mass  
253 of the gas.

254 To assess the performance of a membrane in term of the mass of gas that permeates through  
255 its matrix, Shahrabi et al. [33] describe the gas permeate flux ( $J$ ) ( $\text{kg}/\text{m}^2\text{hr}$ ) through the  
256 membrane as:

$$257 \quad J = \frac{m}{A \cdot t} \quad (3)$$

258 Where  $m$  (g) is the total mass of the permeate at the experimental time interval,  $t$  (h), and  $A$  is  
259 the effective membrane area for permeation ( $\text{m}^2$ )

260 The mass transfer across a gas/membrane/gas system consists of three distinct stages. In this  
261 work, the stages are (1) mass transfer of gas across the gas boundary layer in the porous  
262 medium (2) the transfer of gas through the membrane, (3) transfer of gas across the gas  
263 boundary layer in the open space between the membrane and the pressure transducer  
264 (sensor). Each of these stages acts as a resistance to mass transfer. For a non-porous  
265 membrane, the total resistance ( $1/K_T$ ) can be expressed in series sum of the above resistances:

$$266 \quad \frac{1}{K_T} = \frac{1}{k_{g1}} + \frac{1}{k_m} + \frac{1}{k_{g2}} \quad (4)$$

267 Where  $K_T$ ,  $k_{g1}$ ,  $k_m$ , and  $k_{g2}$  are the mass transfer coefficients for overall, gas boundary in the  
268 porous medium, gas permeation through the membrane, and the gas boundary in the  
269 measurement chamber of membrane-sensor system, respectively. In this work, it can be  
270 assumed that the resistances in the gas boundary layer in the porous medium ( $1/k_{g1}$ ) and in the  
271 open space between the membrane and the sensor ( $1/k_{g2}$ ) are negligible. Thus, we define that  
272  $K_T \cong k_m$ . This assumption is reasonable considering that the gas transfer in the porous medium  
273 was rapid because of the automatic pressure regulation from the supercritical fluid pump, which  
274 imposed constant pressure on the domain throughout the experiment. De Bo [36] similarly  
275 assumes the overall mass transfer resistance in gas/membrane/gas system is equivalent to the  
276 resistance in the non-porous membrane, like the one used in this work. The resistance to pure  
277 gas in the membrane can be determined from the Eq. (5) [37]:

$$278 \quad \frac{1}{k_m} = \frac{\delta}{P} \quad (5)$$

279 Calculations in this work using the Eq. (2) and (3) extend over the entire duration of the  
280 experiments. This approach enables understanding of the response of the membrane–sensor  
281 system from the beginning of gas permeation through the membrane. The primary aim of this  
282 work is to understand the response of the membrane-sensor system at simulated different  
283 geological depths in the event of the  $\text{CO}_2$  leakage from a storage reservoir and to establish a  
284 suitable distinguishing criterion with which a membrane-sensor system can be programmed to



285 detect different gases that permeate through a non-porous membrane in the porous media at  
286 different depths. Therefore, it is important to know the response of the membrane-sensor  
287 system at the start of the permeation, which can be used to characterise the gas leakage  
288 detection.

289 In all experiments, constant pressure and temperature were maintained on the porous domain.  
290 As mentioned earlier, the main driving force for the gas permeation through the membrane was  
291 the difference between the domain pressure and the pressure in the membrane-sensor system,  
292 i.e.,  $p_1-p_0$ .

### 293 **3. Results and discussions**

294 In this section, the responses of the membrane-sensor system to the different imposed  
295 conditions of CO<sub>2</sub> and N<sub>2</sub> are discussed in the context of various parameters, which may affect  
296 the leakage/migration of CO<sub>2</sub> from a storage aquifer. As mentioned earlier, for each experiment,  
297 simultaneous double pressure readings were taken from the two pressure transducers located  
298 at the opposite sides of the centre of the porous domain. Arithmetic average of these readings  
299 was reported for each experiment in this work. Typical behavior of the membrane-sensor  
300 system is shown in Fig. 4 for CO<sub>2</sub> permeation into the membrane at conditions corresponding to  
301 the 250m depth (see, Tab. 2). The simultaneous readings of the two sensors (PTs) are close,  
302 having the maximum standard deviation of 4.7bar. For all experiments, the standard deviations  
303 of the simultaneous sensors' readings reduce with the decreasing depth. At 200 and 50m  
304 depths, the standard deviations are 2.8 and 0.9bar, respectively. The figure also shows that the  
305 domain pressure, which was imposed from the CO<sub>2</sub> pump, remained constant till the end of the  
306 experiment. In some experiments, the gas may leak through connections at the tubing joints,  
307 which seems to arise due to the high pressure of the system. This resulted in the decline of the  
308 pump and domain pressure. Results from such experiments were discarded.

#### 309 **Figure 4**

### 310 **3.1 Gas permeation in the membrane**

311 The permeation of gas through the membrane is recorded as a change in the pressure reading  
312 of the pressure transducer. Using the Van der Waals gas equation, the pressure reading was  
313 used to determine the mass of the gas that has penetrated through the silicon rubber. The  
314 volume of the measurement chamber between the membrane and the sensor in the steel holder  
315 is known. This volume is constant and it is occupied by permeated gas under different  
316 conditions. In all experiments, no significant deformation of the membrane is visible. Therefore,  
317 the volume of the measurement chamber can be confidently assumed constant. The mass of  
318 the gas that permeates the membrane is an important parameter since it is known that the

319 mass is conserved. Mass of  $N_2$  that permeated into the membrane is shown in Fig.5 at the  
320 conditions corresponding to the depths of 150 and 300m. Under these conditions, the figure  
321 shows that the time of the detection of the  $N_2$  (i.e., start of the rise in the mass of the gas) is not  
322 significantly different for the two conditions. It takes more than an hour for any significant mass  
323 of  $N_2$  gas to be recorded. In Fig.6, the responses of the membrane-sensor system to the  
324 presence of  $CO_2$  at different conditions corresponding to different geological depths are shown.  
325 The rate of change of mass of  $CO_2$  increases with depth. This can be seen as the effect of  
326 increasing pressure and temperature with depth. Comparing Figs. 5 and 6, it can be seen that  
327 under similar conditions, the level of the response of the system to the presence of  $CO_2$  far  
328 outweighs that of  $N_2$ . Fig.7 displays this comparison clearly. At the same depth (150m),  
329 significant amount of  $CO_2$  is detected at less than 10 minutes compared to detection of  $N_2$ ,  
330 which takes more than 1 hour. This shows the quick response of the membrane-sensor system  
331 to the presence of  $CO_2$ . Observations above are similar to the findings of many authors on the  
332 high permeation rate of  $CO_2$  in the silicone rubber membrane (see, e.g.,[21], [38], [39], [42–44]).

333 **Figure 5**

334 **Figure 6**

335 **Figure 7**

### 336 **3.2 Dynamic gas flux across the membrane**

337 The dynamic flux of gas across the membrane is calculated using Eq. (3). The dynamic gas flux  
338 across the membrane is plotted against the mass of the permeated gas in order to show the  
339 influence of the driving force on the flux profile. As mentioned earlier, the driving force is the  
340 pressure difference across the membrane. The mass of the gas in the membrane-sensor  
341 system is proportional to the pressure reading by the pressure transducer. Therefore, the plot of  
342 the gas flux against mass of permeated gas informs well about the profile of the gas flux in  
343 relation to the change in the driving force. Flux across the membrane with the permeation of  $N_2$   
344 is shown in Fig.8. Several stages can be discerned in the flux profile of the gas. In the first part  
345 of the curve (Fig.8, 300m depth), the gas flux increases rapidly with the mass of permeated gas.  
346 This continues until the second stage is reached where the increase in gas flux persists but at a  
347 reduced rate than the first stage. This is succeeded by the third stage, which is characterised by  
348 virtually constant flux regime. These three stages can be discerned at 300m depth in Fig. 8. In  
349 the figure, owing to the short duration of the experiment at 150m depth, only the first stage and  
350 part of the second stage are depicted.

351 Fig.9 shows the existence of further stage in the profile of gas flux into the membrane with  $CO_2$ .  
352 Here, we have higher permeation rate for the  $CO_2$ . This enables us to see the behavior of the  
353 flux profile more readily. Following the third stage that was characterised by virtually constant

354 flux of the gas into the membrane (see, Fig. 8), it is clear in Fig.9 that the fourth stage of the  
355 profile is characterised by a decline in flux for all the conditions investigated. Thus, the third  
356 stage represents the peak value of the flux following which there is gradual decline in the gas  
357 flux.

358 Figures 8 and 9 show that the flux of the permeated gas increases with the depth. The value of  
359 the dynamic gas flux recorded with CO<sub>2</sub> on the silicone rubber far outweighs that of N<sub>2</sub> under  
360 similar conditions. The results show that CO<sub>2</sub> diffuses faster through the silicone membrane  
361 than N<sub>2</sub>. Reasons for the decline in the flux profile with the mass of the permeated gas can be  
362 explained in term of the driving force, which is defined to be the difference in pressures across  
363 the membrane. It will be recalled that the increase in the mass of the gas that permeates  
364 through the membrane actually signifies increase in the pressure of the permeated gas in the  
365 measurement chamber of the membrane-sensor system. Thus, increase in the mass of the  
366 permeated gas increases the pressure in the measurement chamber of the membrane-sensor  
367 system. Since the pressure in the porous domain remains constant throughout the experiment,  
368 the increase in the pressure on the side of the membrane-sensor system leads to the decrease  
369 in the driving force. Since the driving force reduces with increase in mass of the permeated gas,  
370 the dynamic gas flux profile continues to decline, as shown in the Figures 8 and 9. Zimmer et al.  
371 [21] calculated the CO<sub>2</sub> gas flux through silicone rubber and found that the flux values increase  
372 with the partial pressure of CO<sub>2</sub>. However, their approach was different from this work as they  
373 only calculated the flux value at a steady state in gas permeation. They also show that the flux  
374 of CO<sub>2</sub> increases with temperature. The trends in their results conform with our findings (shown  
375 in Fig.9) for CO<sub>2</sub> flux values at different depths, corresponding to different pressure and  
376 temperature. The figure shows that the flux values increase with depth.

377 **Figure 8**

378 **Figure 9**

379

### 380 **3.3 Distinguishing criterion for permeated gas**

381 From the foregoing discussions of the results, it is possible to deduce the distinctive criterion to  
382 identify the presence of different gases that permeated through the silicone rubber membrane in  
383 the porous media, using the membrane-sensor system. For CO<sub>2</sub> and N<sub>2</sub> considered in this work,  
384 wide differences in flux and mass of gas permeated are scrutinised. Since mass is conserved  
385 irrespective of the measurement chamber volume under different temperature and pressure, the  
386 rate of change of mass of the permeated gas in the system was considered. This is very  
387 feasible since the rate of mass permeation of CO<sub>2</sub> through the membrane is more than 10 times  
388 higher than that of N<sub>2</sub> under similar conditions. Thus, the slope (i.e., mass permeation rate)

389 obtained from mass versus time curves at various depths can be used to obtain needed model.  
390 The model/equation obtained will be useful in the programming of the membrane-sensor  
391 system to uniquely detect the presence of a gas and possibly alert investigators to the presence  
392 of gas in the measurement chamber. The rate of permeation of the gas through the membrane  
393 was obtained from the slope of the linear equation fitted to the initial permeation stage of the  
394 mass versus time curve. For the CO<sub>2</sub> and N<sub>2</sub> at 150m depth, the mass permeation rates are 2 x  
395 10<sup>-6</sup> and 2 x 10<sup>-7</sup> kg hr<sup>-1</sup>, respectively. The rate was determined from the portion of the mass  
396 permeation versus time curve, where the permeation became noticeable, i.e., at the initial stage  
397 of permeation. This stage of permeation was chosen because the response of the membrane-  
398 sensor system, at this point, is related to the early detection of the subsurface gas or leakage  
399 from the gas storage reservoir. Thus, programming the membrane-sensor system with  
400 parameters obtained at this crucial stage is advantageous for the quick detection of gas leakage  
401 in the subsurface. The mass permeation rate of CO<sub>2</sub> is one degree of order higher than that of  
402 N<sub>2</sub> at the 150m depth. The trends are similar at other corresponding depths. Thus, the presence  
403 of CO<sub>2</sub> can be detected if the gradient of the mass with time recorded by the system is around 2  
404 x 10<sup>-6</sup> kg hr<sup>-1</sup> at the 150m depth. For CO<sub>2</sub> at the other geological depths, Fig.10 shows the  
405 variation of the mass permeation rate with depth for the two gases considered in this work. The  
406 data points are fitted to power law models, which provide the means of predicting the behavior  
407 at various depths.

408 **Figure 10**

409 The above method is useful in the early detection of CO<sub>2</sub> migration or leakage from geological  
410 reservoirs. Early detection at depth will allow for more time to tackle technical tasks before the  
411 CO<sub>2</sub> arrives in shallow groundwater or the earth's surface [21]. In application, alarm system can  
412 be triggered to signify the presence of CO<sub>2</sub>, if the mass permeation rate follows the power law  
413 model provided in Fig.10. This equation can be used to program the membrane-sensor system.  
414 The analysis above shows that the CO<sub>2</sub> has unique mass permeation rate that is different from  
415 that of N<sub>2</sub>. This can also be said of other gases found in the porous media. As shown, this rate  
416 is a function of depth. With the relation of the mass permeation rate to geological depth, using  
417 power law equation, this work has shown that the membrane-sensor system can be used to  
418 monitor gas leakage under different geological conditions. Thus, at any depth, the system can  
419 be applied to give unique indication of gas present. From a practical point of view, one may  
420 wonder whether membrane-sensor system can be successfully applied at deep geological  
421 sediment. The work of Lamert et al. [45] demonstrated the field measurements of electrical  
422 parameters to monitor the subsurface CO<sub>2</sub> movement by installing several copper electrodes at  
423 various depths up to 18.5m below the ground level around the CO<sub>2</sub> injection aquifer. This  
424 enables the investigators to monitor the movement of injected CO<sub>2</sub> in the space surrounding the  
425 injection aquifer. From this practical applications of sensors at depth by Lamert et al. [45], it is

426 believed that miniaturised pressure sensor with membrane can be used for monitoring at  
427 various depths. Abidoeye and Bello [49] also demonstrated how a dielectric model can be  
428 employed in the subsurface monitoring of CO<sub>2</sub> movement. Thus, this work offers additional  
429 possibility in the monitoring for safety of geological carbon sequestration.

430 However, further efforts will be needed to improve on this study. For example, the miniaturised  
431 sensor can be configured with the membrane for better application. Also, future work should  
432 require similar characterization for other gases found in the subsurface, in order to obtain a  
433 broad spectrum of mass permeation rates for different gases for complete programming of  
434 membrane-sensor system. Future work should also include the field application of the  
435 membrane sensor system.

#### 436 **4. Conclusion**

437 The potential of silicone rubber in the monitoring of gas migration in porous media has been  
438 demonstrated using responses of the membrane-sensor system in terms of the mass of  
439 permeated gas and the dynamic gas flux across the membrane are reported for both CO<sub>2</sub> and  
440 N<sub>2</sub>. The results showed the existence of distinguishable stages of permeation for the gases. In  
441 term of the gas flux across the membrane, the first stage involves rapid rise in the flux across  
442 the membrane. This was followed by the less rapid stage of flux, where the gradient reduces  
443 and was succeeded by the stage of constant flux for a period, before the gas flux finally started  
444 to decline because of the reduction in the driving force across the membrane. The results  
445 differed considerably for the two gases with CO<sub>2</sub> flux occurring at higher degree of order than  
446 that of N<sub>2</sub>, under similar conditions. The mass permeation with time for N<sub>2</sub> was more than ten  
447 times less than that for the CO<sub>2</sub>. Based on the mass permeation rate for the different gases,  
448 simple criterion for distinguishing the presence of the gases at various geological depths using  
449 the membrane-sensor system was derived. The power law model was formulated for each gas  
450 to serve as the distinguishing criterion in the monitoring of the subsurface gas migration.

#### 451 **5. Acknowledgement**

452 The authors acknowledge the PhD sponsorship granted by Petroleum Technology  
453 Development Fund (PTDF), Abuja, Nigeria, to one of the authors - Abidoeye, L.K., during which  
454 this work was successfully executed at Loughborough University, UK. The authors are also  
455 grateful to the technologists in Department of Chemical Engineering, Loughborough University,  
456 especially Mr Tony Eyre, for their painstaking efforts in fabricating the complex experimental rig  
457 used in this work.

458

#### 459 **Symbols used**

$J$	Mass flux of gas through the membrane	$\text{kg}(\text{m}^2\text{hr})^{-1}$
$K$	Porous media permeability	$\text{m}^2$
$k_m$	Mass transfer coefficient in the membrane	$\text{ms}^{-1}$
$kg_1$	Mass transfer coefficient in the gas layer on the face of the membrane in the porous domain	$\text{ms}^{-1}$
$kg_2$	Mass transfer coefficient in the measurement chamber of the membrane-sensor system	$\text{ms}^{-1}$
$K_T$	Overall mass transfer coefficient	$\text{ms}^{-1}$
$n$	Number of mole	mol
$p$	Pressure of gas	bar
$m$	Mass of gas	kg
$t$	time	hr
$D_p$	Particle diameter	$\mu\text{m}$
$PT$	Pressure transducer	-
$\phi$	Porosity	-
$\delta$	Thickness of the membrane	m
$V$	Volume of the measurement chamber of the membrane-sensor system	$\text{m}^3$
$T$	System temperature	K
$a$	Van der Waals constant	$\text{kgm}^5\text{s}^{-2}\text{mol}^{-2}$
$b$	Van der Waals constant	$\text{m}^3\text{mol}^{-1}$

460

461

## 462 References

- 463 [1] Chandrappa, R., Gupta, S., and Kulshrestha, U.C., . Coping with climate change:  
464 principles and Asian context, Springer. ISBN 978-3-642-19674-4, 2011.
- 465 [2] Ward, S.E., Ostle, N.J., Oakley, S., Quirk, H., Henrys, P.A., and Bardgett, R.D.  
466 "Warming effects on greenhouse gas fluxes in peatlands are modulated by vegetation  
467 composition," *Ecology letters*, vol. 16, no. 10, pp. 1285–1293, 2013.
- 468 [3] Abidoye, L.K., Das, D.B. and Khudaida, K. Geological carbon sequestration in the  
469 context of two-phase flow in porous media: A review. *Critical Reviews in Environmental Science*  
470 *and Technology*, 45(11), pp. 1105-1147 DOI: 1080/10643389.2014.924184 2014.
- 471 [4] Itaoka, K., Saito, A. and Akai, M.. Public acceptance of CO<sub>2</sub> capture and storage  
472 technology: a survey of public opinion to explore influential factors. In *Proceedings of the*  
473 *7. international conference on greenhouse gas control technologies*, Vancouver, BC  
474 (Canada); 5-9 Sep 2004
- 475 [5] Klapper, R., Widdicombe, S. and Reitz, A. "ECO2 Briefing Paper No. 2: Potential impacts  
476 of CO<sub>2</sub> leakage from sub-surface storage on seabed biology," 2013.
- 477 [6] Krause, R.M., Carley, S. R., Warren, D. C., Rupp, J. A., and Graham, J. D.. Not in (or  
478 Under) My Backyard: Geographic proximity and public acceptance of carbon capture and  
479 storage facilities. *Risk Analysis*, 34(3), pp.529–540., 2014

- 480 [7] Taku Ide, S., Jessen, K. and Orr Jr, F.M. "Storage of CO<sub>2</sub> in saline aquifers: Effects of  
481 gravity, viscous, and capillary forces on amount and timing of trapping," *International*  
482 *Journal of Greenhouse Gas Control*, vol. 1, no. 4, pp. 481–491, 2007.
- 483 [8] Berg, S and Ott, H. "Stability of CO<sub>2</sub>-brine immiscible displacement," *International*  
484 *Journal of Greenhouse Gas Control*, vol. 11, pp. 188–203, Nov. 2012.
- 485 [9] Tao, Q and Bryant, S.L. "Well permeability estimation and CO<sub>2</sub> leakage rates,"  
486 *International Journal of Greenhouse Gas Control*, vol. 22, pp. 77–87, Mar. 2014.
- 487 [10] Gasda, S.E., Nordbotten, J.M. and Celia, M.A. "Vertical equilibrium with sub-scale  
488 analytical methods for geological CO<sub>2</sub> sequestration," *Computational Geosciences*, vol.  
489 13, no. 4, pp. 469–481, 2009.
- 490 [11] Saripalli, K.P., Mcgrail, B.P. and White, M.D. "Modeling the sequestration of CO<sub>2</sub> in deep  
491 geological formations," in *First National Conference on Carbon Sequestration*, no. 509,  
492 pp. 1–19, 2001
- 493 [12] Saraji, S., Goual, L., Piri, M. and Plancher, H, "Wettability of supercritical carbon  
494 dioxide/water/quartz systems: simultaneous measurement of contact angle and  
495 interfacial tension at reservoir conditions.," *Langmuir: the ACS journal of surfaces and*  
496 *colloids*, vol. 29, no. 23, pp. 6856–6866, Jun. 2013.
- 497 [13] Al-Garni , M.T. and Al-Anazi, B.D. "Investigation of wettability effects on capillary  
498 pressure, and irreducible saturation for Saudi crude oils, using rock centrifuge," *Oil and*  
499 *Gas Business*, vol. 2008, no 2, 2008.
- 500 [14] Chiquet, P., Broseta, D. and Thibeau, S. "Wettability alteration of caprock minerals by  
501 carbon dioxide," *Geofluids*, vol. 7, no. 2, pp. 112–122, May 2007.
- 502 [15] Espinoza, D.N., Kim, S.H., and Santamarina, J.C. "CO<sub>2</sub> geological storage —  
503 Geotechnical implications," *KSCE Journal of Civil Engineering*, vol. 15, no. 4, pp. 707–  
504 719, Apr. 2011.
- 505 [16] Nakatsuka, Y., Xue, Z., Garcia, H. and Matsuoka, T. "Experimental study on CO<sub>2</sub>  
506 monitoring and quantification of stored CO<sub>2</sub> in saline formations using resistivity  
507 measurements," *International Journal of Greenhouse Gas Control*, vol. 4, no. 2, pp. 209–  
508 216, 2010.
- 509 [17] Charpentier, F. Bureau, B. Troles, J. Boussard-Plédel, C. Michel-Le Pierrès, K.,  
510 Smektala, F. and Adam, J.-L. "Infrared monitoring of underground CO<sub>2</sub> storage using  
511 chalcogenide glass fibers," *Optical Materials*, vol. 31, no. 3, pp. 496–500, 2009.
- 512 [18] Bielinski, A., Kopp, A., Schütt, H., and Class, H. "Monitoring of CO<sub>2</sub> plumes during  
513 storage in geological formations using temperature signals: Numerical investigation,"  
514 *International Journal of Greenhouse Gas Control*, vol. 2, no. 3, pp. 319–328, 2008.
- 515 [19] Vilamajó, E., Queralt, P., Ledo, J. and Marcuello, A. "Feasibility of Monitoring the  
516 Hontom{ }n (Burgos, Spain) CO<sub>2</sub> Storage Site Using a Deep EM Source," *Surveys in*  
517 *Geophysics*, vol. 34, no. 4, pp. 441–461, 2013.
- 518 [20] Spangler, L.H., Dobeck, L.M. Repasky, K.S. Nehrir, A.R. Humphries, S.D., Barr, J.L.,  
519 Keith, C.J., Shaw, J.A., Rouse, J.H. and Cunningham, A.B. "A shallow subsurface  
520 controlled release facility in Bozeman, Montana, USA, for testing near surface CO<sub>2</sub>

- 521 detection techniques and transport models,” *Environmental Earth Sciences*, vol. 60, no.  
522 2, pp. 227–239, 2010.
- 523 [21] Zimmer, M., Erzinger, J. and Kujawa, C. “The gas membrane sensor (GMS): A new  
524 method for gas measurements in deep boreholes applied at the CO<sub>2</sub>SINK site,”  
525 *International Journal of Greenhouse Gas Control*, vol. 5, no. 4, pp. 995–1001, Jul. 2011.
- 526 [22] Zhang, H. and Cloud, A. “The permeability characteristics of silicone rubber,” in  
527 *Proceedings of the 2006 SAMPE Fall Technical Conference“ Global Advances in*  
528 *Materials and Process Engineering”, Coatings and Sealants Section, 2006.*
- 529 [23] Barnes, A.C., Dejuan Jr, E., Humayun, M., Shelley, T. and Varner, S.E. “Devices for  
530 intraocular drug delivery.” Google Patents, 2012.
- 531 [24] Lazik, D., Ebert, S., Leuthold, M. Hagenau, J. and Geistlinger, H. “Membrane Based  
532 Measurement Technology for in situ Monitoring of Gases in Soil,” *Sensors (Basel,*  
533 *Switzerland)*, vol. 9, no. 2, pp. 756–67, Jan. 2009.
- 534 [25] Cheng, J. and Luo, Y. “Modeling Atmosphere Composition and Determining Explosibility  
535 in a Sealed Coal Mine Volume,” *Archives of Mining Sciences*, vol. 59, no. 1, pp. 25–40,  
536 2014.
- 537 [26] Bednarek, A., Szklarek, S. and Zalewski, M. “Nitrogen pollution removal from areas of  
538 intensive farming—comparison of various denitrification biotechnologies,” *Ecohydrology*  
539 *& Hydrobiology*, vol. 14, no. 2, pp. 132–141, 2014.
- 540 [27] Best, M.G. *Igneous and Metamorphic Petrology*. John Wiley & Sons, 2013.
- 541 [28] Nordbotten, J.M., Celia, M.A. and Bachu, S. “Analytical solutions for leakage rates  
542 through abandoned wells,” *Water Resources Research*, vol. 40(4), Apr. 2004.  
543 DOI:10.1029/2003WR002997
- 544 [29] Das, D.B., Gill, B.S., Abidoye, L.K. and Khudaida, K.J. “A numerical study of dynamic  
545 capillary pressure effect for supercritical carbon dioxide-water flow in porous domain,”  
546 *AIChE Journal*, DOI 10.1002/aic.14577 (in press). 2014.
- 547 [30] Abidoye, L.K. and Das, D.B. pH, Geoelectrical and Membrane Flux Parameters for the  
548 Monitoring of Water-Saturated Silicate and Carbonate Porous Media Contaminated by  
549 CO<sub>2</sub>. *Chemical Engineering Journal*, 262, pp. 1208–1217, 2015.. [31] Bear, J.  
550 *Dynamics of fluids in porous media*. Courier Dover Publications, 2013.
- 551 [32] Hosseini, S.A., Lashgari, H., Choi, J.W., Nicot, J.-P, Lu, J. and Hovorka, S.D. “Static  
552 and dynamic reservoir modeling for geological CO<sub>2</sub> sequestration at Cranfield,  
553 Mississippi, U.S.A.,” *International Journal of Greenhouse Gas Control*, vol. 18, pp. 449–  
554 462, Oct. 2013.
- 555 [33] Salehi Shahrabi, S., Mortaheb, H.R., Barzin, J. and Ehsani, M.R. “Pervaporative  
556 performance of a PDMS/blended PES composite membrane for removal of toluene from  
557 water,” *Desalination*, vol. 287, pp. 281–289, Feb. 2012.
- 558 [34] Baker, R.W. *Membrane Technology and Applications*, 3rd ed. John Wiley & Sons, , p.  
559 592., 2012.
- 560 [35] Van Amerongen, G.J. “Diffusion in elastomers,” *Rubber Chemistry and Technology*, vol.  
561 37, no. 5, pp. 1065–1152, 1964.



- 562 [36] De Bo, I. "Investigation of the permeability and selectivity of gases and volatile organic  
563 compounds for polydimethylsiloxane membranes," *Journal of Membrane Science*, vol.  
564 215, no. 1–2, pp. 303–319, Apr. 2003.
- 565 [37] Ozturk, B. and Hughes, R. "Evaluation of mass transfer characteristics of non-porous  
566 and microporous membrane contactors for the removal of CO<sub>2</sub>," *Chemical Engineering*  
567 *Journal*, vol. 195–196, pp. 122–131, Jul. 2012.
- 568 [38] Kesson, J. "The diffusion of gases through a silicon rubber membrane and its application  
569 to an in-line carbonation meter. MBAA Technical Quarterly 21 (3), 143–146.," *MBAA*  
570 *Technical Quarterly*, vol. 21, no. 3, pp. 143–146, 1984.
- 571 [39] Staude, E. "Membranen und Membranprozesse," *VCH Weinheim*, p. 325 pp., 1992.
- 572 [40] Praveen, J.H.A., Mason, L.W., and Way, J.D. "Characterization of silicon rubber  
573 membrane materials at low temperature and low pressure conditions" *Journal of*  
574 *Membrane Science*, vol. 272, pp. 125–136, 2006.
- 575 [41] Merkel, T.C., Gupta, R.P., Turk, B.S. and Freeman, B.D. "Mixed-gas permeation of  
576 syngas components in poly (dimethylsiloxane) and poly (1-trimethylsilyl-1-propyne) at  
577 elevated temperatures," *Journal of Membrane Science*, vol. 191, no. 1, pp. 85–94, 2001.
- 578 [42] Egli, S., Ruf, A. and Buck, A. "Gastrennung mittels Membranen. Ein Überblick," *Swiss*  
579 *Chem*, vol. 6, no. 9, pp. 89–122, 1984.
- 580 [43] Praveen, J.H.A., Mason, L.W., and Way, J.D. "Characterization of silicon rubber  
581 membrane materials at low temperature and low pressure conditions," *Journal of*  
582 *Membrane Science*, vol. 272, pp. 125–136, 2006.
- 583 [44] Merkel, T.C., Gupta, R.P. Turk, B.S. and Freeman, B.D. "Mixed-gas permeation of  
584 syngas components in poly (dimethylsiloxane) and poly (1-trimethylsilyl-1-propyne) at  
585 elevated temperatures," *Journal of Membrane Science*, vol. 191, no. 1, pp. 85–94, 2001.
- 586 [45] Lamert, H., Geistlinger, H., Werban, U., Schütze, C., Peter, A., Hornbruch, G., Schulz,  
587 A., Pohlert, M., Kalia, S., Beyer, M. and others, "Feasibility of geoelectrical monitoring  
588 and multiphase modeling for process understanding of gaseous CO<sub>2</sub> injection into a  
589 shallow aquifer," *Environmental Earth Sciences*, vol. 67, no. 2, pp. 447–462, 2012.
- 590 [46] Ampomah, W., Balch, R., Grigg, R.B., Cather, M., Gragg, E., Will, R.A., White, M.,  
591 Moodie, N. and Dai, Z. Performance assessment of CO<sub>2</sub>-enhanced oil recovery and  
592 storage in the Morrow reservoir. *Geomechanics and Geophysics for Geo-Energy and*  
593 *Geo-Resources*, 3(3), pp.245-263, 2017.
- 594 [47] Rathnaweera, T.D., Ranjith, P.G. and Perera, M.S.A. Experimental investigation of  
595 geochemical and mineralogical effects of CO<sub>2</sub> sequestration on flow characteristics of  
596 reservoir rock in deep saline aquifers. *Scientific reports*, 6, p.19362., 2016.
- 597 [48] Xiao, T. Dai, Z., McPherson, B., Viswanathan, H. and Jia, W. Reactive transport  
598 modeling of arsenic mobilization in shallow groundwater: impacts of CO<sub>2</sub> and brine  
599 leakage. *Geomechanics and Geophysics for Geo-Energy and Geo-Resources*, 3(3),  
600 pp.339-350, 2017.
- 601 [49] Abidoye, L.K. and Bello, A.A. Simple dielectric mixing model in the monitoring of CO<sub>2</sub>  
602 leakage from geological storage aquifer. Accepted in *Geophysical Journal International*,  
603 208(3), pp. 1787-1795, 2017. doi: 10.1093/gji/ggw495.

604

605

606

607

608

609

610

611

612

613

614 **Tab. 1:** Bulk properties of silica sand used in our experiments

Permeability, $K$ ( $m^2$ )	$3.65 \times 10^{-10}$
Porosity, $\phi$	0.37
Particle Density ( $kg/m^3$ )	2740
Average Particle Diameter, $D_p$ ( $\mu m$ )	946.1
SiO <sub>2</sub> content (%)	99 <sup>a</sup>

615 <sup>a</sup> [www.sibelco.co.uk](http://www.sibelco.co.uk) (accessed May 2014)

616

617

618

619

620

621 **Tab. 2:** List of Experimental Conditions and State of CO<sub>2</sub>

<b>Depth (m)</b>	<b>Domain Temperature (°C)</b>	<b>Domain/Injection Pressure (bar)</b>
50	22.25	13.5
150	26.75	40.5
200	29	54
250	31.25	67.5

622

623

624

625

626

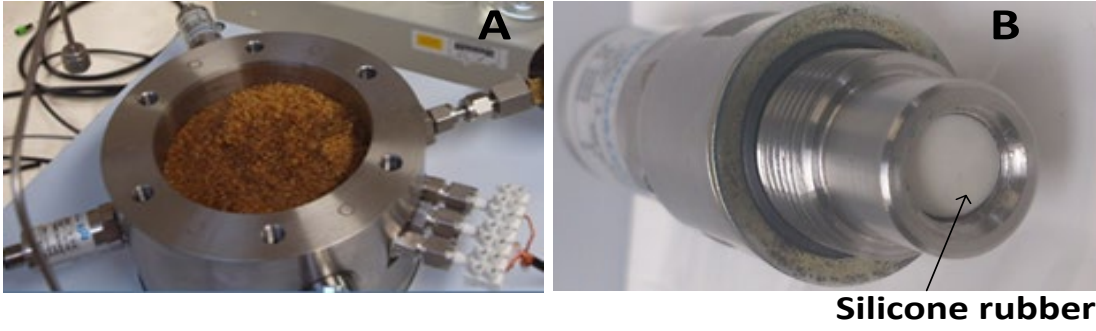
627

628

629

630

631



632

633 Fig 1:

634

635

636

637

638

639

640

641

642

643

644

645

646

647

648

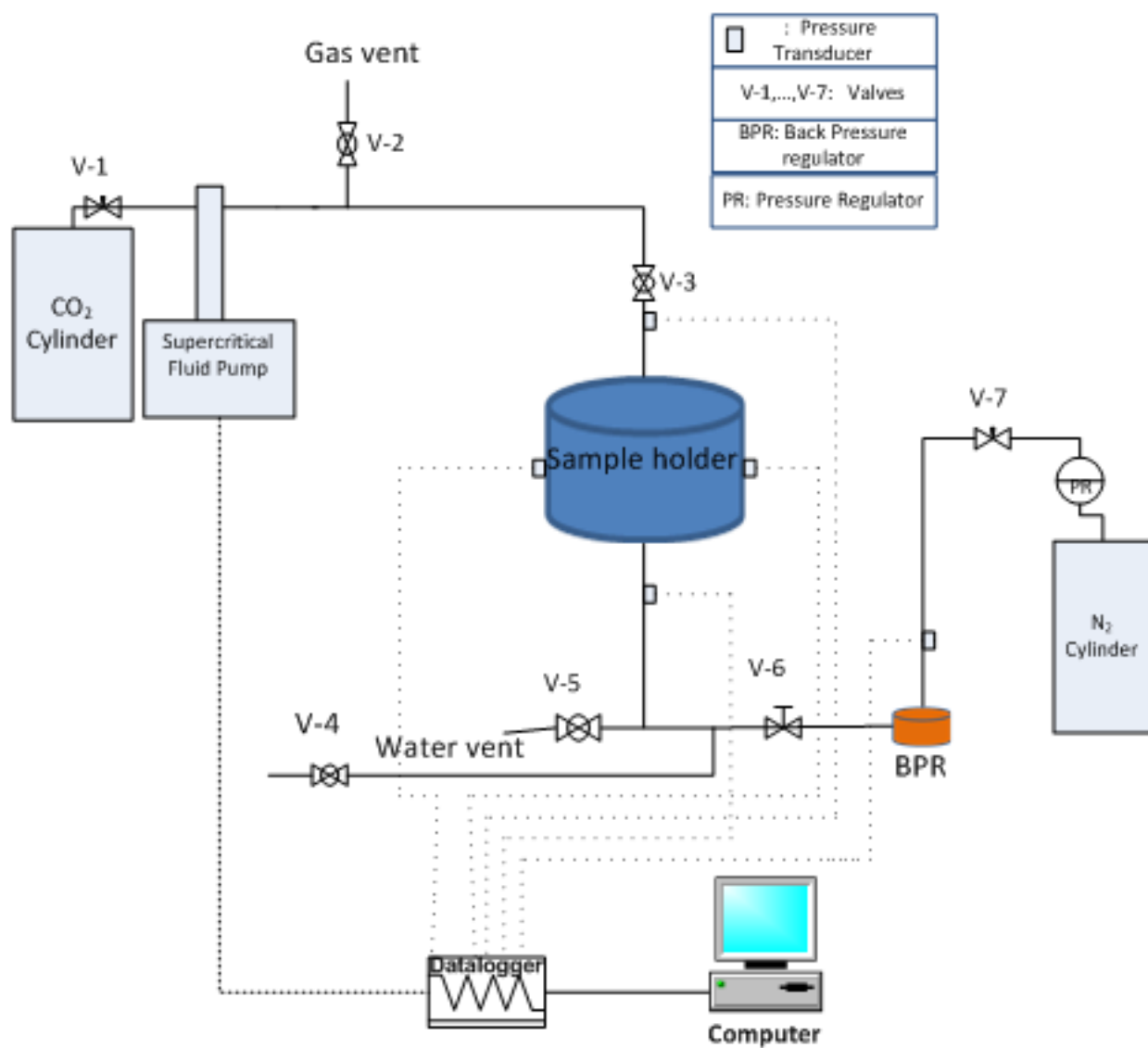
649

650

651

652

653



654

655 Fig. 2

656

657

658

659

660

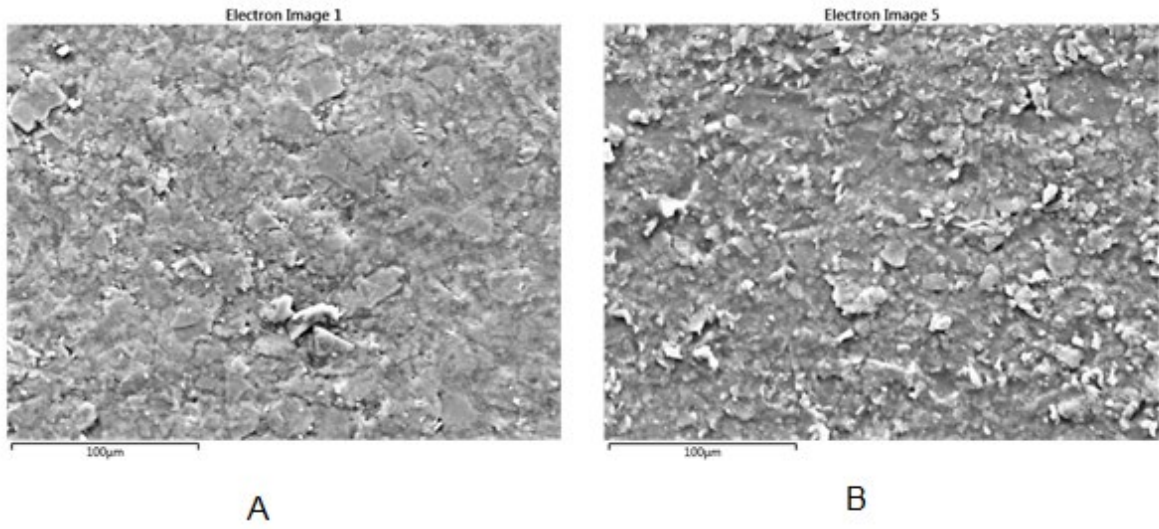
661

662

663

664

665  
666  
667  
668

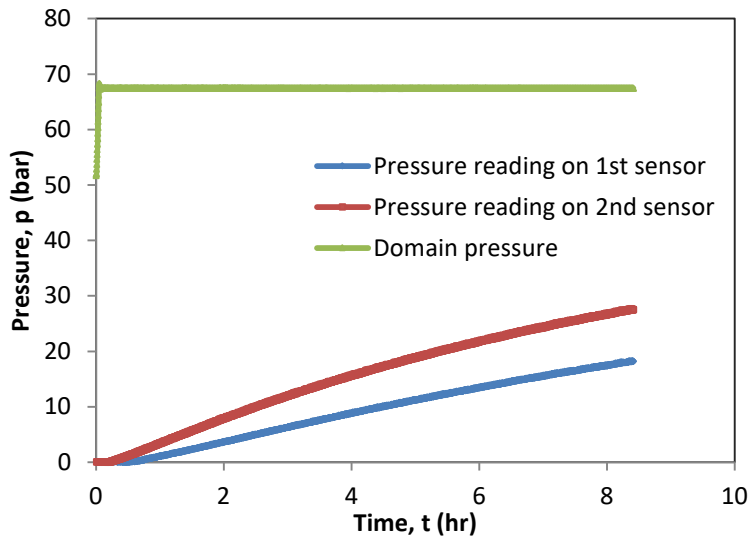


669

Fig. 3

670  
671  
672  
673  
674  
675  
676  
677  
678  
679  
680  
681  
682  
683  
684

685  
686  
687  
688



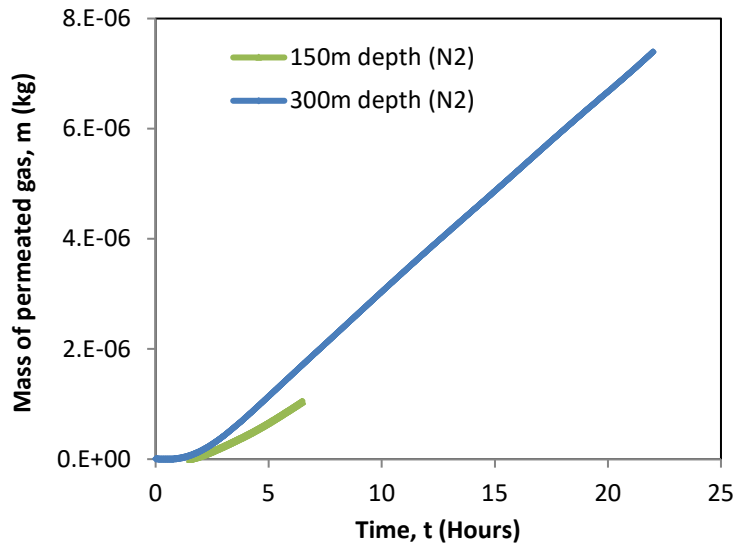
689

Fig. 4

690  
691  
692  
693  
694  
695  
696  
697  
698  
699  
700  
701  
702  
703  
704



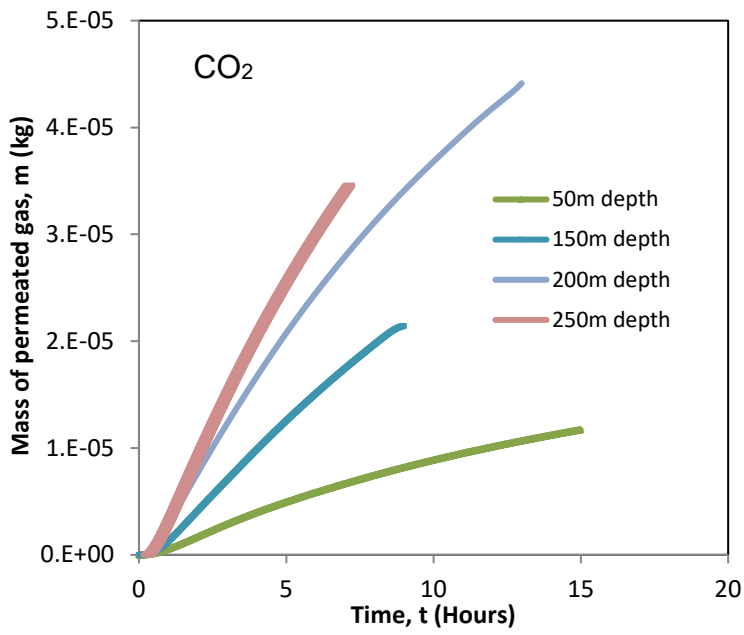
705  
706  
707  
708  
709



710  
711 Fig. 5

712  
713  
714  
715  
716  
717  
718  
719  
720  
721  
722

723  
724  
725  
726  
727

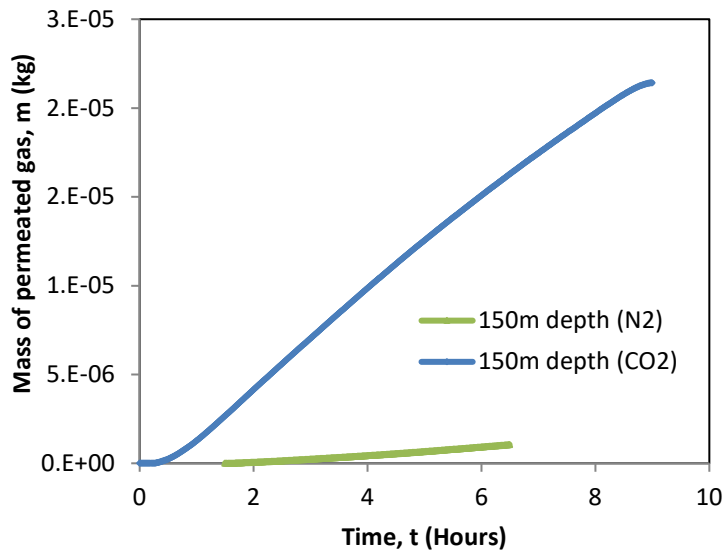


728

729 **Fig. 6**

730  
731  
732  
733  
734  
735  
736  
737  
738  
739  
740  
741

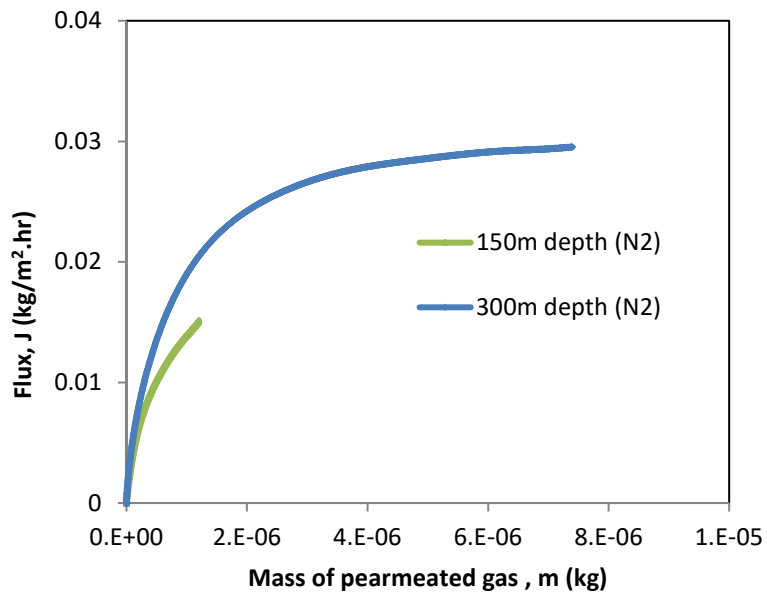
742  
743  
744  
745  
746  
747



748  
749  
750  
751  
752  
753  
754  
755  
756  
757  
758  
759  
760  
761

Fig. 7

762  
763  
764  
765  
766



767

768 Fig. 8

769

770

771

772

773

774

775

776

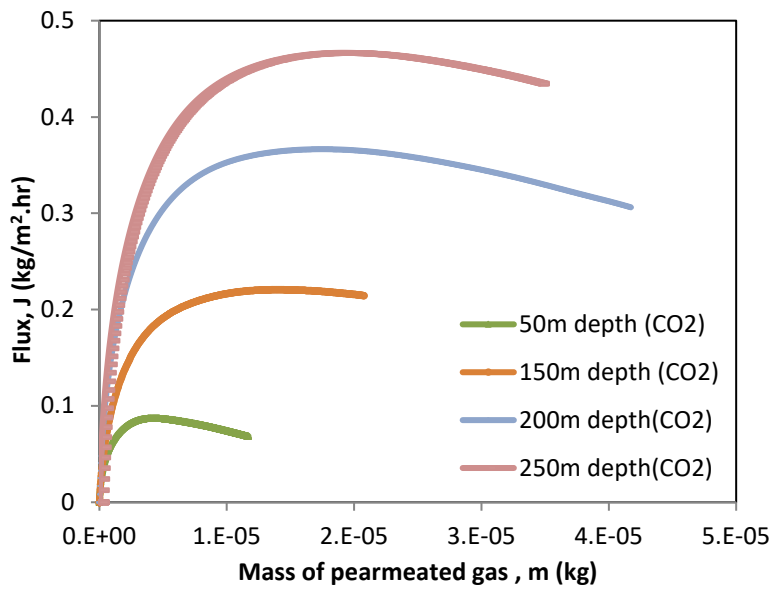
777

778

779

780

781  
782  
783  
784  
785



786

787 Fig. 9

788

789

790

791

792

793

794

795

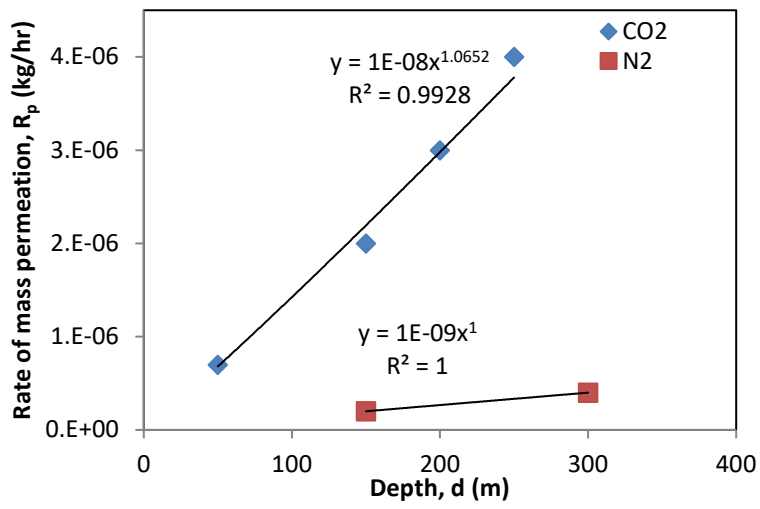
796

797

798

799

800  
801  
802  
803  
804



805

806 Fig. 10

807

808

809

810

811

812

813

814

815

816

817

818

819

820

821

822

823

824 **Fig.1:** Photographs of (A) The sample holder showing silica sand and pressure transducer (B)  
825 Membrane-sensor system: Steel holder holds the pressure transducer at the rear and the  
826 silicone rubber sheet at the front (metal cap not shown). Sample holder size: internal  
827 diameter=10cm, sample height=4cm

828

829 **Fig.2:** High-pressure experimental set-up for the investigation of gas migration in the porous  
830 media using membrane-sensor system

831

832 **Fig.3:** Scans of (A) Fresh (B) Used (experiment at 67.5 bar, 31.25°C, i.e., 200m depth) silicone  
833 rubber membrane using FEGSEM (LEO 1530VP, Carl Zeiss SMT, Oberkochen, Germany)

834

835 **Fig.4:** Simultaneous responses of the two pressure transducers to the CO<sub>2</sub> gas that permeated  
836 through the membrane at imposed conditions corresponding to 250m depth. Plots identification  
837 for black and white print: Top plot (domain pressure), Middle plot (2<sup>nd</sup> sensor), Bottom plot (1<sup>st</sup>  
838 sensor)

839

840 **Fig.5:** Mass of permeated gas (N<sub>2</sub>) under conditions that mimic different depths. Upper plot(  
841 300m depth), lower plot (150m depth)

842

843 **Fig.6:** Mass of permeated gas (CO<sub>2</sub>) through the membrane under conditions that mimic  
844 different depths. Uppermost (250m depth), 2<sup>nd</sup> plot (200m), 3<sup>rd</sup> plot (150m), lowermost plot(50m  
845 depth)

846

847 **Fig.7:** Mass of permeated gases (CO<sub>2</sub> and N<sub>2</sub>) through the membrane under similar conditions.  
848 Upper plot (CO<sub>2</sub>), lower plot (N<sub>2</sub>)

849

850 **Fig.8:** Change in the flux of permeated gas (N<sub>2</sub>) under conditions that mimic different depths.  
851 Upper plot (300m depth), lower plot (150m depth)

852

853 **Fig.9:** Change in the flux of permeated gas (CO<sub>2</sub>) under conditions that mimic different depths. .  
854 Uppermost (250m depth), 2<sup>nd</sup> plot (200m), 3<sup>rd</sup> plot (150m), lowermost plot(50m depth)



855

856

857 **Fig.10:** Models of mass permeation rate for different gases at different geological depths for  
858 application in the distinction of the presence of the different gases in the porous medium.

859

860

861